SCIENCE CHINA
Information Sciences

March 2023, Vol. 66 130304:1–130304:20
https://doi.org/10.1007/s11432-022-3626-5

• REVIEW •
Special Topic: Spectrum, Coverage, and Enabling Technologies for Intelligent 6G

Reconfiguring wireless environments via intelligent surfaces for 6G: reflection, modulation, and security

Jindan XU[1], Chau YUEN[1*], Chongwen HUANG[2], Naveed UL HASSAN[3], George C. ALEXANDROPOULOS[4,6], Marco DI RENZO[5] & Mérouane DEBBAH[6]

[1]*Engineering Product Development Pillar, Singapore University of Technology and Design, Singapore* 487372, *Singapore;*
[2]*College of Information Science and Electronic Engineering, Zhejiang University, Hangzhou* 310007, *China;*
[3]*Department of Electrical Engineering, Lahore University of Management Sciences, Lahore* 54792, *Pakistan;*
[4]*Department of Informatics and Telecommunications, National and Kapodistrian University of Athens, Athens* 15784, *Greece;*
[5]*Université Paris-Saclay, CNRS, CentraleSupélec, Laboratoire des Signaux et Systèmes, Gif-sur-Yvette* 91192, *France;*
[6]*Technology Innovation Institute, Masdar City* 9639, *United Arab Emirates*

Received 23 August 2022/Revised 22 October 2022/Accepted 16 November 2022/Published online 20 February 2023

Abstract The reconfigurable intelligent surface (RIS) has been recognized as an essential enabling technology for sixth-generation (6G) mobile communication networks. An RIS comprises a large number of small and low-cost reflecting elements whose parameters can be dynamically adjusted with a programmable controller. Each of these elements can effectively reflect a phase-shifted version of the incident electromagnetic wave. By configuring the wave phases in real time, the propagation environment of the information-bearing signals can be dynamically manipulated to enhance communication reliability, boost transmission rate, expand cellular coverage, and strengthen communication security. In this study, we provide an overview on RIS-assisted wireless communications. Specifically, we elaborate on the state-of-the-art enabling techniques for the RIS technology as well as their corresponding substantial benefits from the perspectives of RIS reflection and RIS modulation. With these benefits, we envision the integration of RISs into emerging applications for 6G. In addition, communication security is of unprecedented importance in future 6G networks with ubiquitous wireless services in multifarious verticals and areas. We highlight potential contributions of RISs to physical-layer security, in terms of secrecy rate and secrecy outage probability, exemplified by a typical case study from both theoretical and numerical aspects. Finally, we discuss challenges and opportunities on the deployment of RISs in practice to motivate future research.

Keywords reconfigurable intelligent surface, physical-layer security, RIS-assisted wireless communications, phase modulation, 6G

Citation Xu J D, Yuen C, Huang C W, et al. Reconfiguring wireless environment via intelligent surfaces for 6G: reflection, modulation, and security. Sci China Inf Sci, 2023, 66(3): 130304, https://doi.org/10.1007/s11432-022-3626-5

1 Introduction

Owing to the high data traffic and massive connections for vertical applications, e.g., Internet-of-Everything (IoE), integrated sensing and communications (ISAC), and space-air-ground-ocean (SAGO) communications, in future wireless networks, the sixth-generation (6G) mobile communication network is expected to provide extremely superior performance compared to the fifth-generation (5G) network. Specifically, the key performance indicators (KPIs) of 6G require to support wireless communications with peak data rate in the order of Tbps, user-experienced data rate upto 1 Gbps, 100 GHz maximum bandwidth, etc. [1]. To meet these stringent requirements, it is a widely-recognized path toward 6G to further evolve the massive multiple-input multiple-output (MIMO) technology and deeply explore the high-frequency spectrum.

* Corresponding author (email: yuenchau@sutd.edu.sg)

By exploiting hundreds, or even thousands, of antennas to perform beamforming, the hardware cost and power consumption of massive MIMO increase exponentially with the number of antennas [2–4]. As a potential cost-effective and energy-efficient solution, reconfigurable intelligent surface (RIS) has recently attracted much attention and has been regarded as an evolutionary extension of massive MIMO [5–10]. Specifically, an RIS consists of a large number of small and low-cost passive reflecting elements whose parameters are dynamically reconfigurable with a programmable controller [11]. Each of these elements can effectively reflect a phase-shifted version of the incident electromagnetic wave. By adjusting the wave phases in real time, the propagation environment is dynamically reconfigured to enhance communication efficiency [12–20], expand cellular coverage [21–23], and strengthen communication security [24–31]. These potentials of RIS in the physical layer also inspire the feasibility design of medium access control (MAC) to enable multiple-device communications with the assistance of RISs [32,33]. Unlike the existing technology of amplify-and-forward relay [34–36], RIS requires no radio frequency (RF) chains and performs as a passive array which does not have the ability of signal processing. Since this passive array surface induces negligible power consumption, it is easy for RIS to be integrated into wireless environments, e.g., by being deployed into ceilings, building facades, etc. However, the multiplicative fading of the cascade channels via the RISs limits the capacity gain in many scenarios [37]. To overcome this limitation, the concept of active RIS has been proposed in [38], where the RIS elements can not only reflect but also amplify the incident signals via integrated amplifiers.

On the other hand, the 6G KPI in terms of transmission rate ranging from Gbps upto Tbps requires large bandwidth, which is only available in the high-frequency spectrum, e.g., millimeter-wave (mm-Wave), terahertz (THz), and visible light (VL) frequency bands. Compared to the popularly adopted sub-6 GHz spectrum, high-frequency electromagnetic radiation experiences high free-space loss and severe oxygen absorption. Due to these effects, communication in these high-frequency bands is dominated by highly directional line-of-sight (LoS) links [39]. Such communications are vulnerable to blockage by various obstacles, such as walls, furniture, humans, and vehicles, especially in complicated indoor and dense urban environments [40]. RIS is an efficient solution to deal with the vulnerability of high-frequency spectrum by providing additional reflected paths [41–47].

Besides, 6G will support vertical applications, e.g., ISAC and SAGO communications. On one hand, the performance of conventional ISAC is limited, to a large extent, by unfavorable wireless environments, especially for the absence of LoS links using a high-frequency spectrum. RIS can be incorporated into ISAC networks to improve the system performance via efficiently reconfiguring the communication environment [48, 49]. On the other hand, for SAGO applications with satellites, unmanned aerial vehicles (UAVs), ships, and even underwater vehicles, the battery power of terminal devices is generally limited and it is usually inconvenient to frequently replace the built-in batteries. RIS provides an effective solution for enabling energy efficient SAGO transmissions via passive beamforming [50–52].

In addition, communication security has attracted vast interest for 6G networks [53, 54]. With ubiquitous wireless services in multifarious areas, communications are becoming more vulnerable to eavesdropping and we are going to face unprecedented security issues in 6G networks [55, 56]. In most current applications, the security is guaranteed by using encryption techniques which rely on the assumption of relatively limited computation ability of eavesdroppers. However, it has been initially motivated by the landmark discovery in [57] that strictly secure communications are difficult from the physical layer. Techniques of this kind, namely physical-layer security, are designed by exploiting physical-layer characteristics like the properties of wireless channels. Particularly in [58], for the first time, the physical-layer security has been shown possible for an application to mm-Wave channels by developing a practical secure transmission scheme in the beam domain. Exploring this high-frequency spectrum, RIS can naturally be utilized to reconfigure the propagation environment so that the physical-layer security is enhanced by improving the communication reliability of legitimate terminals while suppressing the leakage of information to eavesdroppers.

In this paper, we give an overview on RIS-assisted wireless communications for 6G networks. Specifically, we focus on two main functionalities of RISs, i.e., reflection and modulation, and elaborate on the state-of-the-art enabling techniques from these two perspectives. We show that RIS provides a cost-and-power efficient solution for coverage extension and rate boosting. Thanks to these benefits, we envision opportunities for integrating RISs with a wide variety of emerging applications, including high-frequency transmissions, ISAC, and SAGO communications. Besides, we evince the paramount importance of security in 6G networks and highlight the contributions of RIS to guarantee secure communications at the physical layer. In particular, RIS is capable of enhancing the secrecy performances in terms of secrecy

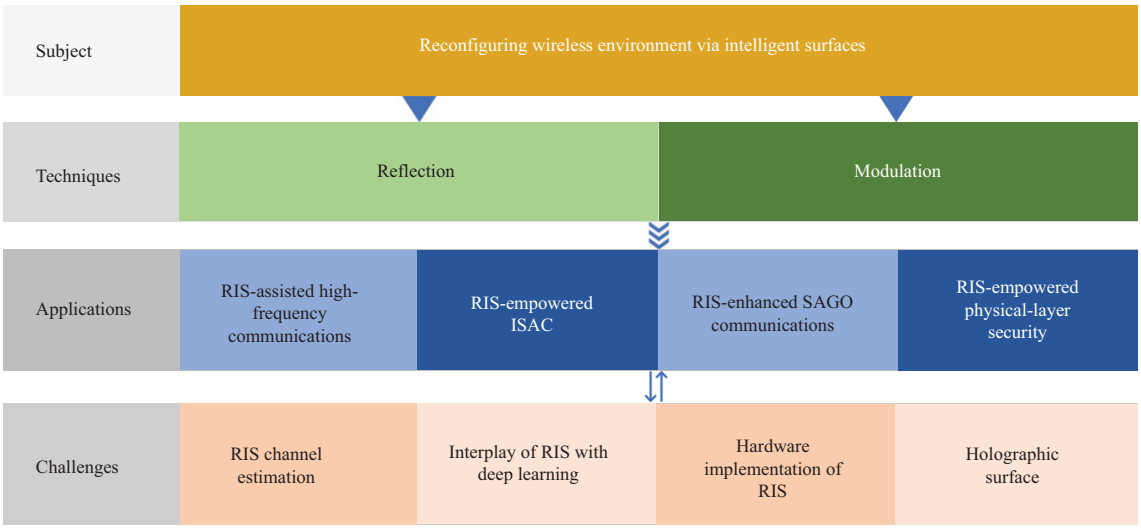

Figure 1 (Color online) The organization of this study.

rate and secrecy outage probability (SOP). Finally, we point out a multitude of challenging open issues for further research. The organization of this paper is illustrated in Figure 1.

The rest of this paper is organized as follows. In Section 2, we elaborate on RIS reflection and RIS modulation, and expose their corresponding benefits for wireless communications. In Section 3, we discuss opportunities for integrating RIS with emerging 6G applications. Due to the importance of security in 6G networks, we elaborate in Section 4 on the contributions of RIS to physical-layer security, exemplified by a case study. In Section 5, we point out several prominent challenges and opportunities for further research. Conclusions are drawn in Section 6.

2 RIS reflection and modulation

In order to reap the potential benefits of RIS, there are two main ways for utilizing an RIS for communication performance enhancement, as illustrated in Figure 2. In particular, an RIS can serve as a reflector to reflect the incident electromagnetic wave via superimposed passive beamforming. Alternatively, an RIS can operate as a transmitter which carries additional information via phase modulation schemes. In this section, we discuss these essential enabling techniques as well as their corresponding benefits from the perspectives of RIS reflection and modulation.

2.1 RIS reflection with instantaneous CSI

As a typical reflection feature of RIS, energy efficient passive beamforming has been intensively investigated in existing studies [18–23, 59–68]. It helps improve the communications in two ways. On the one hand, RIS reflection can establish virtual LoS paths to expand the cell coverage. On the other hand, the received signal power can be enhanced via RIS beamforming. However, the achievable performance realized by RIS-assisted communications, especially with massive MIMO, is usually limited by various hardware impairments, e.g., discrete phase shifts, imperfect channel state information (CSI), low-resolution analog-to-digital converters, and limited RF chains. These constraints of hardware impairments are critical factors in the design of cost-and-power efficient RIS communication systems in practice.

One of these constraints is that RIS can typically apply a finite number of discrete adjustable phase shifts. In [18], the discrete phase shifts for the RIS have been jointly designed with the transmit power for each user, in order to maximize the energy efficiency in a multiuser multiple-input single-output (MISO) system. It is revealed that RIS-assisted communications, even with coarse 1-bit phase shifts, significantly outperform traditional relay-assisted communications in terms of energy efficiency. The impact of phase errors at the RIS and imperfect RF chains at the base station (BS) have been characterized in [19], which has shown that the spectral efficiency saturates due to hardware impairments even when the numbers of elements at both the RIS and BS grow infinitely. A hybrid beamforming method has been proposed

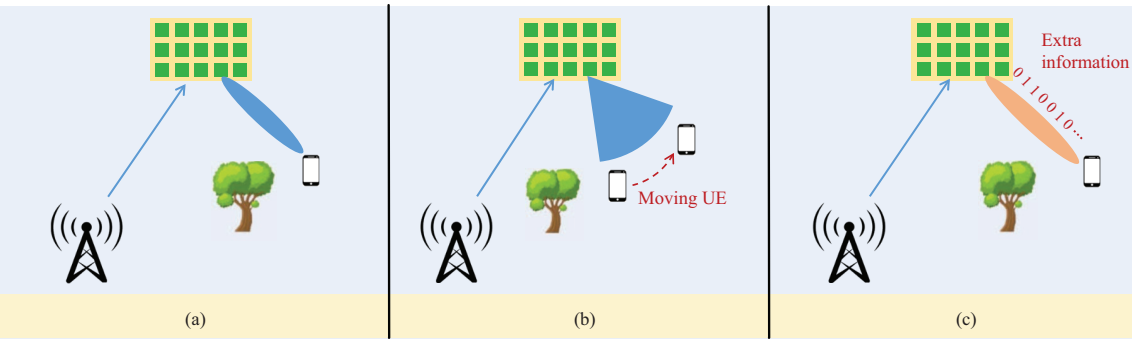

Figure 2 (Color online) RIS reflection and modulation. (a) RIS reflection with instantaneous CSI; (b) RIS reflection with statistical CSI; (c) RIS-phase modulation.

in [20], considering discrete analog beamforming at the RIS and continuous digital beamforming at the BS for sum rate maximization.

In addition, it is usually difficult to acquire CSI especially in RIS-assisted communication systems. This is because an RIS is a nearly passive device with no ability to transmit or receive RIS-specific pilots. In order to tackle this challenge, a robust optimization scheme of passive RIS beamforming with imperfect CSI has been developed in [59]. In [60], a general framework for the robust transmission design of an RIS-assisted multiuser MISO system has been proposed. Specifically, a transmit power minimization problem has been formulated subject to the worst-case rate constraints with imperfect CSI at the transmitter. In addition, a joint channel estimation and signal detection algorithm has been proposed in [61] to simultaneously estimate the CSI and the transmitted signals.

2.2 RIS reflection with statistical CSI

As discussed in previous text, it is difficult to acquire perfect CSI. Besides, the pilot and computation overhead to acquire instantaneous CSI in an RIS-aided channel may be unaffordable in some scenarios, e.g., in high mobility setups and when the reflecting surface has a very large number of elements. To tackle these challenges, some efforts have been devoted to studying the coverage extension [21–23], reflection optimization [63–65], and joint beamforming design [66–68] in RIS-assisted systems by utilizing statistical CSI as illustrated in Figure 2(b).

By exploiting statistical CSI, a closed-form expression of the coverage area has been derived in [21], which quantitatively demonstrates that an RIS can extend the network coverage. Assuming statistical CSI for RIS optimization, a closed-form expression for the coverage probability has been derived in [22]. The obtained analytical framework shows that the coverage probability scales up with N^2 where N is the number of reflecting elements of the RIS. Moreover, a quasi-static broad coverage has been designed in [23] by exploiting statistical CSI. Considering the overhead for channel estimation, it has been verified that the proposed quasi-static broad coverage may outperform RIS designs based on instantaneous CSI.

In an RIS-assisted MISO communication system, the RIS reflection coefficients based on statistical CSI have been optimized to maximize the ergodic spectral efficiency [63]. To compensate for the performance loss due to the lack of instantaneous CSI, a balanced choice of quantization resolution for the phase shifts has been proposed, leading to a cost-effective system design. In addition, an RIS-aided multi-pair communication system has been investigated in [64], assuming the availability of statistical CSI. An expression of the achievable rate has been derived and a genetic algorithm has been proposed for continuous and discrete phase shift designs. Based on statistical channel correlation information and considering imperfect CSI, the authors of [65] have proposed an RIS reflection method for distributed RISs. Moreover, the theoretical ergodic rate analysis done in [65] has unveiled that a distributed RIS deployment may outperform a centralized architecture with the same number of total reflecting elements.

The absence of instantaneous CSI introduces challenges to the joint optimization of RIS beamforming and BS precoding. Utilizing statistical CSI in Rician fading, the authors of [66] have proposed an iterative algorithm to solve the joint optimization problem in an RIS-assisted MISO communication system. In [67], a joint beamforming algorithm has been proposed for RIS-assisted MIMO systems by exploiting only the second-order momentum of the channel statistics. Specifically, the passive beamforming at the RIS and the transmit covariance matrix at the BS are alternatively optimized. In [68], a two-timescale

beamforming scheme has been presented, in which the beamforming at the RIS is first optimized based on statistical CSI and the precoding at the BS is then designed based on instantaneous CSI. RIS reflection designs based on statistical CSI provide an effective alternative to achieve a better tradeoff between the overhead for channel estimation and the achievable performance, especially in highly dynamic wireless environments.

2.3 RIS-phase modulation for rate boosting

Several research studies have confirmed that RIS can increase the coverage and reliability of wireless links. However, it has been recently shown that an RIS can be efficiently utilized as a transmitter as well. Specifically extra information can be transmitted through an RIS by, e.g., by modulating the adjustable phases of the reflecting elements, as illustrated in Figure 2(c) [69].

It has been proved in [70] that the joint encoding of the RIS reflection coefficient and the BS transmission is a capacity-achieving approach in an RIS-assisted communication system. RIS-aided schemes with reflection modulation have been shown to outperform existing schemes where the RIS acts as a pure reflector [71]. In [72], it has been revealed that the degrees of freedom of RIS-assisted MIMO channels can be improved by using RIS-phase modulation. Based on an ON/OFF reflection modulation scheme, a simultaneous passive beamforming and information transfer (PBIT) scheme for multiuser MIMO communications has been proposed in [73]. A sample average approximation-based iterative algorithm has been developed for beamforming, while a turbo message passing algorithm has been proposed to solve the bilinear estimation problem at the receiver. Since the reflected signal power fluctuates over time with the number of ON reflecting elements, the outage probability of PBIT can be high. As a remedy, an RIS-based reflection pattern modulation (RIS-RPM) scheme has been proposed in [74], in which a subset of reflecting elements is switched on to implement efficient beamforming at the cost of conveying less amount of information via the RIS. In these ON/OFF RIS-phase modulation schemes, the reflected power is less than the maximum power since only some reflecting elements are switched on. To prevent this excessive power loss, quadrature reflection modulation (QRM) methods have been proposed in [75, 76] where all RIS elements remain active. In [75], the reflecting elements are partitioned into two subsets according to the local transmit data at the RIS. The phase shifts of the first subset are utilized for RIS reflection, while the second subset is configured ensuring orthogonality with the first subset, i.e., adding a phase shift equal to $\frac{\pi}{2}$. In [76], the RIS is partitioned into two subsets to create signals with only in-phase and quadrature components, respectively. Each subset of the surface is steered towards a receive antenna whose the index carries the bit information. Furthermore, the impact of hardware impairments, including phase-dependent amplitude and discrete phase shift, on the RIS-phase modulation has been analyzed in [77].

By operating as a reflector and transmitter, the RIS can distinctly enhance the transmission rate [70–72]. However, most of the existing joint detectors are based on a maximum likelihood algorithm which is prohibitively complicated. The performance loss caused by linear detectors may not be negligible. Therefore, the design of RIS-phase modulation with low-complexity detection methods deserves further study.

3 Emerging RIS-empowered wireless applications for 6G

Acting either as a reflector or as a transmitter, an RIS enhances the performance of wireless communications via directional beamforming and phase modulation. Thanks to these benefits, RISs have shown great potential for being integrated in numerous applications, some of which have been intensively discussed in overview studies [7, 8, 49]. In this section, we focus on three emerging applications, i.e., high-frequency transmissions, ISAC, and SAGO communications, as illustrated in Figure 3.

3.1 RIS-assisted communications in high-frequency bands

Compared to 5G, 6G calls for order-of-magnitude increments in communication bandwidth in order to fulfill the KPI in terms of the transmission rate. This is only possible when exploring the high-frequency spectrum, e.g., mm-Wave, THz, and even VL frequency bands. However, the path loss of high-frequency electromagnetic waves is usually severe and the LoS connectivity may be compromised

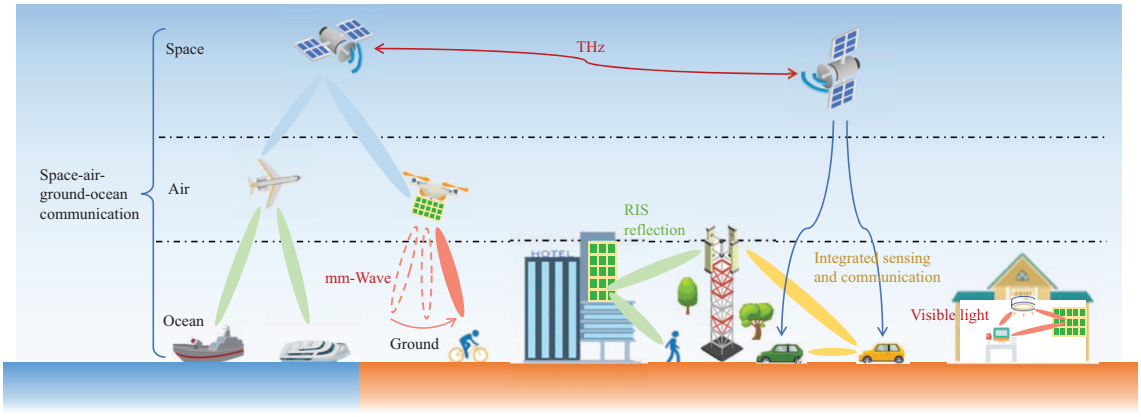

Figure 3 (Color online) Emerging RIS-empowered wireless applications for 6G.

even to the presence of blocking objects. By shaping the wireless environment, an RIS is potentially beneficial to enhancing the communication reliability in the high-frequency spectrum.

In [41], an RIS has been utilized to mitigate the impact of blockages in mm-Wave secure communications. By applying a geometric model for sparse mm-Wave channels, the RIS reflecting and transmit beamforming have been jointly designed via an alternating optimization method. Compared to the mm-Wave radio spectrum ranging from 30 to 300 GHz, the THz band provides more abundant bandwidth, i.e., from 0.1 to 10 THz. However, transmission at the THz band suffers from extremely high free-space losses and is extraordinarily sensitive to blockage. Considering an RIS-assisted THz massive MIMO system, the authors of [42] proposed two beamforming approaches, i.e., narrow beam steering and spatial bandpass filtering, and a closed-loop channel estimation method. Considering multiple RISs deployed to assist multiuser MISO communication, a joint design of analog beamforming at the RISs and digital beamforming at the BS has been proposed in [43]. In addition to the mm-Wave and THz frequencies, VL communication enjoys the advantage of abundant unlicensed optical spectrum [44]. In [45], VL communication has been utilized in an RIS-aided dual-hop indoor system. To be specific, closed-form expressions of the outage probability and bit error rate (BER) have been analyzed and both performance metrics are significantly improved by exploiting an RIS. In addition, the authors of [46] have shown that the integration of RIS with light fidelity technology enables plenty of innovative applications. From these studies on high-frequency applications, it is concluded that RIS plays an important role in combating the large path loss and vulnerability due to blockage in high-frequency communications.

3.2 RIS-empowered integrated sensing and communications

ISAC has attracted great interest from industry and academia for decades due to its manifold applications for object detection, tracking, and positioning [78–86]. Sensing usually refers to estimating the positions and velocities of the targets via the reflected RF signals from the target terminals. On the one hand, reliable virtual LoS links constructed by an RIS improve the positioning accuracy of sensing. An RIS-assisted positioning and communication architecture has been investigated in [78]. Compared to a traditional system without RIS, the proposed scheme achieves up to two orders of magnitude reduction in positioning error. Furthermore, the authors of [79] have characterized the theoretical limits of an RIS-assisted ISAC system based on a general near/far-field signal model. It is revealed that the gain of positioning accuracy benefited from the RIS increases significantly with the carrier frequency.

On the other hand, RIS beamforming can improve the sensing signal-to-noise ratio (SNR) and expand the sensing range [80]. To maximize the minimum beampattern gain towards a desired sensing direction, joint optimization of RIS beamforming and BS precoding has been studied in [82]. Under the constraints of transmit power and communication SNR, the problem of sensing design is nonconvex and an alternating optimization solution has been proposed to optimize the sensing beampattern while guaranteeing the communication SNR requirement. Taking the sensing receiver design into account, an iterative algorithm has been proposed in [83] to improve the communication rate while guaranteeing a minimum sensing SNR.

In addition to the aforementioned sensing techniques, spectrum sensing plays an important role in RIS-empowered ISAC systems. The incident signals on an RIS are usually mixed with interfering signals,

Table 1 RIS-empowered physical-layer security

Secure metrics	Ref.	System setup		Main contribution
Secrecy rate	[24]	Single-user MISO w. single RIS	Single eavesdropper w. single antenna	Jointly optimize RIS phase shifts and transmit signal covariance
	[25]	Single-user MISO w. multiple RISs	Single eavesdropper w. single antenna	Jointly optimize RIS phase shifts and transmit precoding
	[26]	Single-user MIMO w. single RIS	Single eavesdropper w. multiple antennas	Jointly optimize RIS phase shifts, transmit signal covariance, and AN covariance
	[27]	Multiuser MISO w. multiple RISs	Multiple eavesdroppers w. multiple antennas	Jointly optimize RIS phase shifts, transmit signal covariance, and AN covariance with imperfect CSI
	[28]	Single-user MIMO w. legitimate & eavesdropping RISs	Single eavesdropper w. multiple antennas	Jointly optimize RIS phase shifts, legitimate combining matrix, transmit precoding, and AN covariance
Secrecy outage probability	[29]	Single-user SISO w. single RIS	Single eavesdropper w. single antenna	Asymptotic SOP analysis
	[30]	MIMO w. single RIS & randomly located users	Single eavesdropper w. multiple antennas	SOP analysis in closed form and probability analysis of nonzero secrecy capacity
	[31]	Single-user SISO w. single RIS	Multiple cooperative eavesdroppers	Exact SOP analysis under discrete phase shifters

leading to a degraded received signal-to-interference-plus-noise ratio (SINR) at the desired receiver. To address this issue, a trained convolutional neural network (CNN) has been exploited at the RIS controller to infer the interfering signals from the incident signals [84]. By utilizing federated spectrum learning, the wireless bandwidth allocation, user-RIS association, and phase shift configuration have been jointly optimized in [85]. In [86], an RIS framework with intelligent spectrum sensing has been developed to exploit the inherent characteristics of the RF spectrum. All these studies evince enormous potential of RIS in assisting ISAC for 6G communications.

3.3 Space-air-ground-ocean communications with RIS

The concept of SAGO communication is considered to be a key feature of the 6G network which will provide seamless global coverage. The use of RIS enables the energy efficient SAGO transmissions. In [50], an RIS-assisted SAGO architecture has been proposed where multiple RISs are integrated with multiple-access edge computing platforms [51] to improve both communication and computing powers. Besides, an RIS-assisted multiple access framework has been proposed in [52] which offers fairness for different types of terminals while reducing the computational complexity of RISs.

In addition, an RIS can enhance the diversity order when adopted for air communications [87]. In air-RIS systems, an RIS can be deployed on an airplane or a UAV to achieve additional flexibility [88]. As depicted in Figure 3, this technique adds a dimension of mobility to RIS and improves its ability to establish LoS links, especially in terrains lacking infrastructure, e.g., in disaster areas. Furthermore, the extra degree of freedom can be provided by the rotation of the RIS plane [89].

Furthermore, SAGO communications face various unprecedented security risks, including physical, operational, network, and information threats, especially for underwater acoustic communications [90]. RIS reflection helps direct a large amount of signal energy to desired terminals and areas, which in fact contributes to the communication security.

Existing research studies [50, 52, 87–90] show that SAGO communication can take advantage of RIS to enhance the energy efficiency, diversity order, and communication security.

4 RIS-empowered physical-layer security for 6G

The development of cellular networks to 6G aims to serve all vertical applications and to connect things all around the world from ground to space. Communication security is therefore of unprecedented importance. Different from conventional cryptographic methods implemented at the network and application layers [91], physical-layer security ensures secure transmissions from the fundamental perspective of information theory. It is thus robust to the growing computational ability of advanced adversaries. In this section, we elaborate on RIS for physical-layer security from the perspectives of improving the secrecy rate and reducing SOP. Results are illustrated considering a typical case study for RIS-assisted mm-Wave secure communications.

4.1 RIS reflection design for enhanced secrecy rate

The secrecy rate is a fundamental metric of physical-layer security to characterize the ability to prevent private information from eavesdropping [92]. An RIS is capable of enhancing the secrecy rate. For example, an RIS can improve the received signal power at legitimate terminals while suppressing the leakage of information to potential eavesdroppers via beamforming towards desired directions.

The aim to maximize the secrecy rate usually results in a nonconvex optimization problem due to the unit-modulus constraint for the RIS phase shifts and the complex objective of the secrecy rate. In order to find a locally optimal solution to this optimization problem with coupled variables, alternating algorithms have been developed to optimize one variable with the others kept fixed [24–28]. In [24], an alternating algorithm has been proposed to jointly optimize the RIS phase shifts and transmit signal covariance for secrecy rate maximization in an RIS-assisted MIMO system in the presence of a passive eavesdropper equipped with a single antenna. This method can be generalized to a general scenario with a multi-antenna eavesdropper. Then, multiple RISs have been considered in [25] where the RIS beamforming and BS precoding have been jointly optimized. Further in [26], artificial noise (AN) has been adopted in RIS-aided channels to guarantee secure transmissions, where the covariance matrix of the AN has also been jointly optimized with the RIS reflection. This additional optimization variable resulted in an extremely complicated nonconvex problem. To address this issue, the coupled variables were alternately optimized while keeping the secrecy rate non-decreasing. Moreover, practical concerns of imperfect CSI and scenarios with multiple eavesdroppers have been considered in [27], where a robust alternating algorithm has been developed by utilizing the optimization techniques of successive convex approximation and semidefinite relaxation. In addition, an eavesdropping RIS has been taken into account in [28] to assist wiretap. It is revealed that a positive secrecy rate is unachievable in the absence of a legitimate RIS, even for eavesdropping RISs equipped with small numbers of elements. Most of these schemes have reported significant performance gains in terms of the secrecy rate provided that the RIS reflection coefficients are appropriately optimized.

4.2 RIS-empowered communications with reduced secrecy outage

In addition to secrecy rate, SOP, which is defined as the probability that the instantaneous secrecy rate falls below a target threshold, is an alternative popular metric to characterize the performance of physical-layer security [29–31]. Under the assumption of a large number of RIS elements, asymptotic SOP analysis has been conducted in [29] for a basic RIS-assisted secrecy transmission model consisting of a transmitter, a legitimate user, and an eavesdropper. In [30], comprehensive secrecy performance analysis, including both SOP and average secrecy rate, has been presented by comparing RIS-assisted communication to a conventional MIMO system without RIS. Specifically, an exact expression of the SOP has been derived under the assumption of randomly located users by applying stochastic geometry. It is revealed that the secrecy performance in terms of SOP can be significantly improved with an increasing number of RIS elements. Moreover, a closed-form expression of the SOP with phase quantization errors has been derived in [31].

In Table 1, we summarize the studies on RIS configured as a reflector to enhance the secrecy rate and improve the SOP. As discussed in Subsection 2.3, an RIS can also be utilized as a transmitter carrying extra information via phase modulation. This functionality also contributes to secure communications. For example, more private information can be transmitted via RIS-phase modulation to the desired user-equipments (UEs). On the other hand, AN can also be generated via RIS-phase modulation to help jam the eavesdropper. Therefore, it is an interesting problem to investigate the modulation design of RIS for secure communications.

4.3 A case study on RIS-empowered communications

In this subsection, we present a case study on secure mm-Wave communications to explicitly and quantitatively elaborate on the benefits of deploying an RIS for secure communications. Specifically, we study a typical three-terminal wiretap channel, where a multi-antenna transmitter (Alice) sends confidential signals to a desired receiver (Bob) in the presence of an eavesdropper (Eve). Under the assumption that the LoS path between Alice and Bob/Eve is blocked, an RIS is exploited to assist the secure communication as displayed in Figure 4.

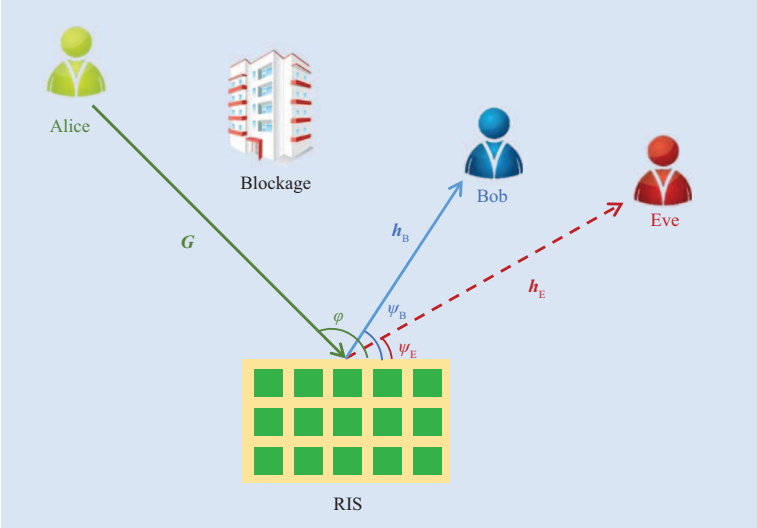

Figure 4 (Color online) A secure mm-Wave communication system assisted with an RIS.

We assume that the RIS is equipped with N reflecting elements while Alice has M antennas. Bob and Eve are single-antenna receivers. Due to the spatial sparsity of mm-Wave MIMO channels, we assume that all the channels in this system are dominated by LoS paths. Let $\boldsymbol{G} = l_{\mathrm{A}}^{\frac{1}{2}}\boldsymbol{g}_{\mathrm{R}}\boldsymbol{g}_{\mathrm{A}}^{\mathrm{H}}$, $\boldsymbol{h}_{\mathrm{B}} = l_{\mathrm{B}}^{\frac{1}{2}}\boldsymbol{g}_{\mathrm{B}}$, and $\boldsymbol{h}_{\mathrm{E}} = l_{\mathrm{E}}^{\frac{1}{2}}\boldsymbol{g}_{\mathrm{E}}$ denote the Alice-RIS, RIS-Bob, and RIS-Eve channels, respectively, where $\boldsymbol{g}_{\mathrm{A}} \in \mathbb{C}^{M\times 1}$, $\boldsymbol{g}_{\mathrm{R}} \in \mathbb{C}^{N\times 1}$, $\boldsymbol{g}_{\mathrm{B}} \in \mathbb{C}^{N\times 1}$, and $\boldsymbol{g}_{\mathrm{E}} \in \mathbb{C}^{N\times 1}$ are signature response vectors[1)], and l_{A}, l_{B}, and l_{E} are the large-scale channel coefficients.

Alice transmits the signal s through the precoder vector $\boldsymbol{w} \in \mathbb{C}^{M\times 1}$. Assuming $\mathbb{E}\left\{|s|^2\right\} = 1$ and $\|\boldsymbol{w}\|^2 = 1$, the received signals at Bob and Eve are

$$y_{\mathrm{B}} = \boldsymbol{h}_{\mathrm{B}}^{\mathrm{H}}\boldsymbol{\Theta}\boldsymbol{G}\sqrt{P}\boldsymbol{w}s + n_{\mathrm{B}}, \tag{1}$$

and

$$y_{\mathrm{E}} = \boldsymbol{h}_{\mathrm{E}}^{\mathrm{H}}\boldsymbol{\Theta}\boldsymbol{G}\sqrt{P}\boldsymbol{w}s + n_{\mathrm{E}}, \tag{2}$$

where $n_{\mathrm{B}} \sim \mathcal{CN}(0, \sigma_n^2)$ and $n_{\mathrm{E}} \sim \mathcal{CN}(0, \sigma_n^2)$ denote the thermal noises at Bob and Eve, respectively, σ_n^2 is the noise power, and $\boldsymbol{\Theta} = \mathrm{diag}\{\mathrm{e}^{\mathrm{j}\theta_1}, \mathrm{e}^{\mathrm{j}\theta_2}, \ldots, \mathrm{e}^{\mathrm{j}\theta_N}\}$ denotes the phase shift matrix at the RIS with θ_i being the phase shift of the ith reflecting element.

4.3.1 *Theoretical secrecy rate analysis*

Consider the secrecy capacity defined in [93] as

$$C_S = \max_{s\to\boldsymbol{w}s\to y_{\mathrm{B}},y_{\mathrm{E}}} I\Big(s; y_{\mathrm{B}}\Big) - I\Big(s; y_{\mathrm{E}}\Big), \tag{3}$$

where $I(\cdot;\cdot)$ denotes the mutual information between two random variables. Adopting a maximal-ratio-transmission (MRT) at Alice, i.e., $\boldsymbol{w} = \frac{(\boldsymbol{h}_{\mathrm{B}}^{\mathrm{H}}\boldsymbol{\Theta}\boldsymbol{G})^{\mathrm{H}}}{\|\boldsymbol{h}_{\mathrm{B}}^{\mathrm{H}}\boldsymbol{\Theta}\boldsymbol{G}\|}$, the achievable secrecy rate is obtained as

$$R_S = \left[\log_2\left(1+\gamma_{\mathrm{B}}\right) - \log_2\left(1+\gamma_{\mathrm{E}}\right)\right]^+, \tag{4}$$

1) Specifically, $\boldsymbol{g}_{\mathrm{A}} = [1, \mathrm{e}^{-\mathrm{j}2\pi\frac{d}{\lambda}\cos\phi}, \ldots, \mathrm{e}^{-\mathrm{j}2\pi(M-1)\frac{d}{\lambda}\cos\phi}]^{\mathrm{T}}$ where $\phi \sim \mathcal{U}(0,\pi)$ is the angle of departure (AoD) of the transmit signal at Alice, d denotes the distance between adjacent antenna elements, and λ denotes the wavelength of the carrier frequency. The vectors $\boldsymbol{g}_{\mathrm{R}}$, $\boldsymbol{g}_{\mathrm{B}}$, and $\boldsymbol{g}_{\mathrm{E}}$ are similarly defined with $\varphi \sim \mathcal{U}(0,\pi)$ denoting the angle of arrival (AoA) at the RIS, $\psi_{\mathrm{B}} \sim \mathcal{U}(0,\pi)$ denoting the AoD of the reflected signals from the RIS to Bob, and $\psi_{\mathrm{E}} \sim \mathcal{U}(0,\pi)$ denoting the AoD of the reflected signals from the RIS to Eve, respectively.

where $[x]^+ = \max\{0, x\}$ returns the maximum of 0 and x;

$$\gamma_{\mathrm{B}} = \frac{P}{\sigma_n^2} \left\| \boldsymbol{h}_{\mathrm{B}}^{\mathrm{H}} \boldsymbol{\Theta} \boldsymbol{G} \right\|^2 = \frac{l_{\mathrm{A}} l_{\mathrm{B}} P}{\sigma_n^2} \left\| \boldsymbol{g}_{\mathrm{B}}^{\mathrm{H}} \boldsymbol{\Theta} \boldsymbol{g}_{\mathrm{R}} \boldsymbol{g}_{\mathrm{A}}^{\mathrm{H}} \right\|^2 = \frac{l_{\mathrm{A}} l_{\mathrm{B}} M P}{\sigma_n^2} \left| \boldsymbol{g}_{\mathrm{B}}^{\mathrm{H}} \boldsymbol{\Theta} \boldsymbol{g}_{\mathrm{R}} \right|^2, \tag{5}$$

and

$$\gamma_{\mathrm{E}} = \frac{P}{\sigma_n^2} \frac{\left| \boldsymbol{h}_{\mathrm{E}}^{\mathrm{H}} \boldsymbol{\Theta} \boldsymbol{G} \boldsymbol{G}^{\mathrm{H}} \boldsymbol{\Theta}^{\mathrm{H}} \boldsymbol{h}_{\mathrm{B}} \right|^2}{\left\| \boldsymbol{h}_{\mathrm{B}}^{\mathrm{H}} \boldsymbol{\Theta} \boldsymbol{G} \right\|^2} = \frac{l_{\mathrm{A}} l_{\mathrm{E}} M P}{\sigma_n^2} \frac{\left| \boldsymbol{g}_{\mathrm{E}}^{\mathrm{H}} \boldsymbol{\Theta} \boldsymbol{g}_{\mathrm{R}} \boldsymbol{g}_{\mathrm{R}}^{\mathrm{H}} \boldsymbol{\Theta}^{\mathrm{H}} \boldsymbol{g}_{\mathrm{B}} \right|^2}{\left| \boldsymbol{g}_{\mathrm{B}}^{\mathrm{H}} \boldsymbol{\Theta} \boldsymbol{g}_{\mathrm{R}} \right|^2} = \frac{l_{\mathrm{A}} l_{\mathrm{E}} M P}{\sigma_n^2} \left| \boldsymbol{g}_{\mathrm{E}}^{\mathrm{H}} \boldsymbol{\Theta} \boldsymbol{g}_{\mathrm{R}} \right|^2, \tag{6}$$

are the received SNRs at Bob and Eve, respectively.

Comparing (5) with (6), the differences between the desired SNR γ_{B} and the leakage SNR γ_{E} come from two aspects. One is the large-scale channel coefficients l_{B} and l_{E}, which depend on the distances between the RIS to Bob and the RIS to Eve, respectively. The other is the beamforming gains $\left| \boldsymbol{g}_{\mathrm{B}}^{\mathrm{H}} \boldsymbol{\Theta} \boldsymbol{g}_{\mathrm{R}} \right|$ and $\left| \boldsymbol{g}_{\mathrm{E}}^{\mathrm{H}} \boldsymbol{\Theta} \boldsymbol{g}_{\mathrm{R}} \right|$, which characterize the cascades channels and the RIS phase shifts. To ensure secure communication, we analyze the secrecy performance assuming the optimal RIS phase shifts to improve γ_{B} while suppressing γ_{E}.

Without the knowledge of the presence of Eve, $\boldsymbol{\Theta}$ is optimized by maximizing the received SNR of Bob as in a conventional RIS communication system. The optimal phase shifts at the RIS to maximize γ_{B} in (5) is therefore $\boldsymbol{\Theta}^* = \mathrm{diag}\{1, \mathrm{e}^{\mathrm{j}\theta}, \ldots, \mathrm{e}^{\mathrm{j}(N-1)\theta}\}$, where $\theta = 2\pi \frac{d}{\lambda} (\cos\varphi - \cos\psi_{\mathrm{B}})$. Substituting $\boldsymbol{\Theta}^*$ into (4), the achievable secrecy rate is evaluated by

$$R_S = \left[\log_2 \left(1 + \frac{l_{\mathrm{A}} l_{\mathrm{B}} M N^2 P}{\sigma_n^2} \right) - \log_2 \left(1 + \frac{l_{\mathrm{A}} l_{\mathrm{E}} M P}{\sigma_n^2} \left| \boldsymbol{g}_{\mathrm{E}}^{\mathrm{H}} \boldsymbol{g}_{\mathrm{B}} \right|^2 \right) \right]^+. \tag{7}$$

In (7), the first term is the achievable rate of Bob given the optimal RIS beamforming while the second term is the eavesdropping rate of Eve. This implies that the transmit power can be scaled down by $\frac{1}{N^2}$ while maintaining a fixed desired rate at Bob. A positive secrecy rate is needed to establish a secure communication link. Two observations are given in the following.

Observation 1. Under the assumptions $l_{\mathrm{B}} \geqslant l_{\mathrm{E}}$ and $N \to \infty$, a tight lower bound for the ergodic achievable secrecy rate R_S in (7) is obtained as

$$\underline{R}_S = \log_2 \left(1 + \frac{l_{\mathrm{A}} l_{\mathrm{B}} M N^2 P}{\sigma_n^2} \right) - \log_2 \left(1 + \frac{l_{\mathrm{A}} l_{\mathrm{E}} M P}{\sigma_n^2} \eta \right), \tag{8}$$

where $\eta \triangleq N - \frac{2}{\pi^2}(N-1) + \frac{2N}{\pi^2}(\ln N + a)$ and a is the Euler's constant.

The proof is given in Appendix A. From (8), the desired SNR at Bob increases with N^2 while the leakage SNR at Eve increases with $N \ln N$. Therefore, an increasing number of reflecting elements is beneficial to the ergodic secrecy rate. The quantitative scaling law is further characterized in the following observation.

Observation 2. For large $N \to \infty$ and $M \to \infty$, the lower bound for the ergodic achievable secrecy rate $\underline{R}_S$ in (8) converges to

$$\underline{R}_S \to \log_2 \left(\frac{N^2 l_{\mathrm{B}}}{\eta l_{\mathrm{E}}} \right) \to \log_2 \left(\frac{N \pi^2 l_{\mathrm{B}}}{2 l_{\mathrm{E}}} \right), \tag{9}$$

where we have applied the relation $\log(1+x) \to \log(x)$ for large $x \to \infty$ and have used the definition of η.

This observation states that the ergodic achievable secrecy rate increases with N while saturating for large M. This is because N reflecting elements at the RIS provide a diversity gain of the order of N^2 for Bob but this is not equally beneficial for Eve. In contrast, increasing the number of antennas at Alice, the transmit beamforming gain is equally improved for both Bob and Eve. Therefore, it is more efficient to increase the number of reflecting elements at the RIS, which is also more energy efficient, than to increase the number of antennas at Alice.

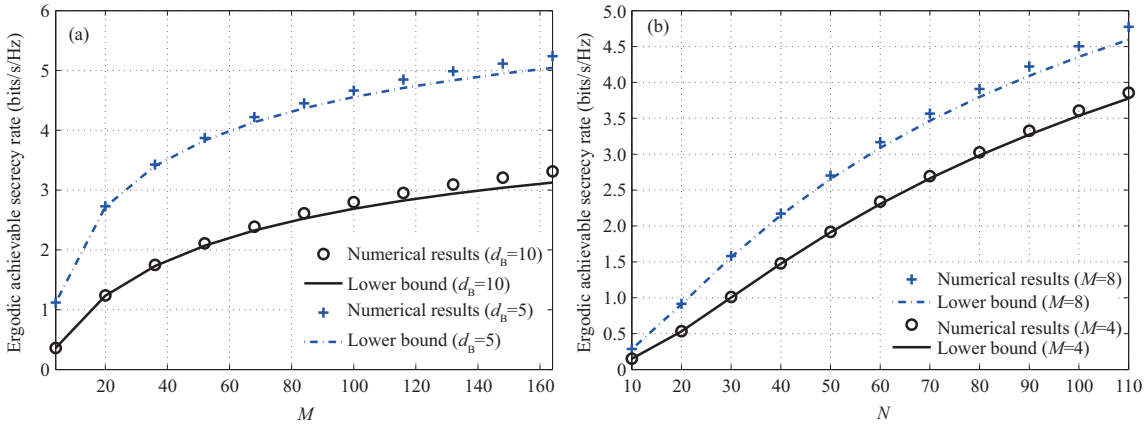

Figure 5 (Color online) Ergodic achievable secrecy rate versus M and N ($\phi = \frac{\pi}{4}$ and $\varphi = \frac{3\pi}{4}$). (a) $N = 8$, $d_{\rm A} = 10$, and $d_{\rm E} = 30$; (b) $d_{\rm A} = 15$, $d_{\rm B} = 20$, and $d_{\rm E} = 30$.

4.3.2 *Numerical simulations*

We set the transmit power as $P = 20$ W, the noise spectral density as -174 dBm/Hz, and the bandwidth as 100 M. We exploit a standard linear model of the free space path loss of l for mm-Wave communications as [39]

$$-10\log_{10}(l) = \alpha + \beta 10\log_{10}(d), \tag{10}$$

where d is the distance in meters, and α and β are respectively the least square fits of the floating intercept and slope over the measured distances. In particular, we set $\alpha = 61.4$ and $\beta = 2$ for 28 GHz [39].

Figure 5 verifies the tightness of the derived lower bound in (8). $l_{\rm A}$, $l_{\rm B}$, and $l_{\rm E}$ denote the distances between the RIS and Alice, Bob, and Eve, respectively. The secrecy rate increases with M and finally saturates as shown in Figure 5(a). A large number of transmit antennas provide more degrees of freedom at Alice, which is equally beneficial to Bob and Eve. Its bonus to the secrecy rate is thus limited. On the other hand, the secrecy rate monotonically increases with N in Figure 5(b). More efficient beamforming toward Bob can be realized by a larger number of reflecting elements at the RIS, making it more challenging for Eve to wiretap.

Consider the particular scenario illustrated in Figure 4, where Bob and Eve are located with AoDs $\psi_{\rm B} \in (0, \frac{\pi}{2})$ and $\psi_{\rm E} \in (0, \frac{\pi}{2})$, respectively. Given that Eve is fixed at a position, we define a secrecy area of Bob where the secrecy rate satisfies $R_S \geqslant R_0$ for a threshold secrecy rate $R_0 \geqslant 0$. The secrecy areas of Bob are illustrated in Figure 6 given a fixed Eve marked by a pentagram. The wheat, green, and black lines are contours of the ergodic secrecy rate corresponding to $R_0 = 1, 2$, and 4 bps/Hz, respectively. In order to guarantee the target secrecy rate, e.g., $R_0 = 1$ bps/Hz illustrated by the wheat line in Figure 6(b), Bob is supposed to be located within 17.3 m to the coordinate origin in the same direction of Eve, i.e., $\psi_{\rm B} = \psi_{\rm E} = \frac{\pi}{4}$. This distance constraint can be relaxed to about 30 m when Bob lies in different directions from Eve, i.e., $|\psi_{\rm B} - \psi_{\rm E}| > \frac{\pi}{12}$. By comparing the subfigures in Figure 6, we observe that the secrecy area can be significantly expanded by increasing the number of RIS-reflecting elements. Similar observations can be obtained from the 3D contours of the secrecy area in Figure 7.

5 Research challenges and opportunities

Emerging as a promising technology for 6G, the deployment of RIS faces a multitude of challenges and opportunities. In this section, we discuss a few challenging issues and potential topics for future research.

5.1 RIS channel estimation

Channel estimation is an essential prerequisite in RIS-assisted communication systems. In the following, we overview state-of-the-art estimation schemes for two different RIS structures, i.e., passive (no power amplification) and semi-passive RISs.

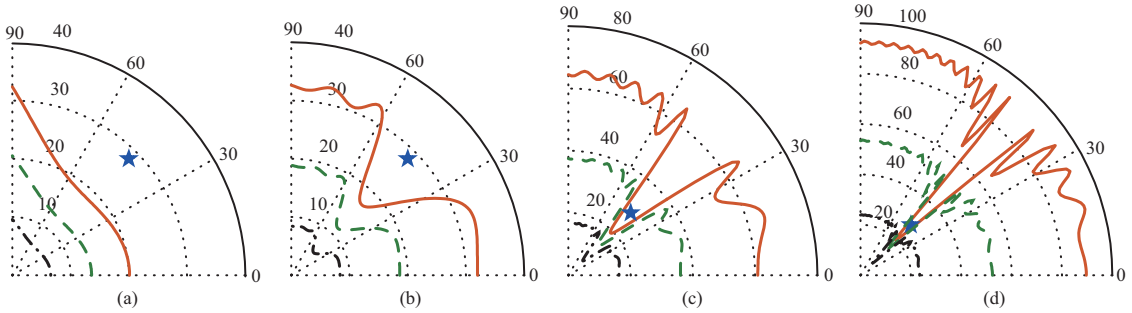

Figure 6 (Color online) Secrecy area ($d_A = 5\sqrt{2}$, $d_{\rm E} = 20\sqrt{2}$, $\psi_{\rm E} = \frac{\pi}{4}$, $\phi = \frac{\pi}{4}$, and $\varphi = \frac{3\pi}{4}$). (a) $M = 1024$, $N = 2$; (b) $M = 32$, $N = 8$; (c) $M = 32$, $N = 16$; (d) $M = 16$, $N = 32$.

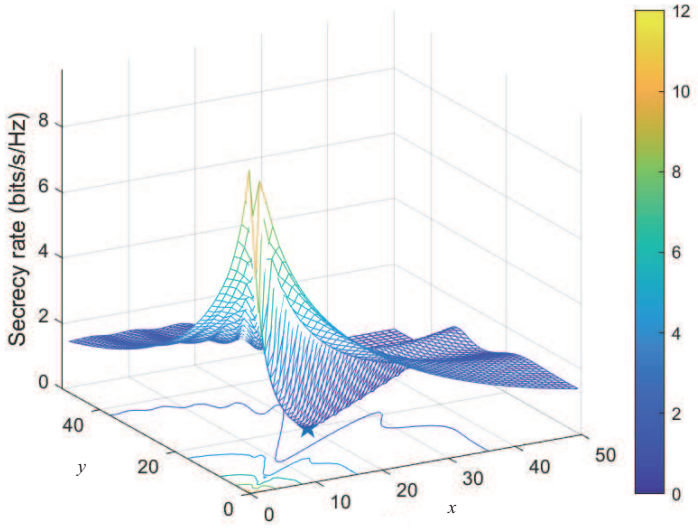

Figure 7 (Color online) 3D contours of the secrecy area ($d_{\rm A} = 5\sqrt{2}$, $d_{\rm E} = 20\sqrt{2}$, $\psi_{\rm E} = \frac{\pi}{4}$, $\phi = \frac{\pi}{4}$, $\varphi = \frac{3\pi}{4}$, $M = 32$, and $N = 16$).

5.1.1 *Channel estimation for passive RIS*

Typically, an RIS is a passive device with no RF chains to actively transmit, receive, and process pilot sequences. However, an RIS needs power to enable the reconfigurability. It is therefore difficult to perform separate channel estimations for the BS-RIS and RIS-UE channels [94, 95]. In addition, the large size of the reflecting array, resulting in a large number of channel coefficients to estimate, also makes the channel estimation extremely challenging.

To estimate the cascaded BS-RIS-UE channel, a straightforward estimation framework is the ON/OFF method, in which the intricate estimation process is divided into multiple sub-phases and only a part of the RIS reflecting elements are switched on in each sub-phase. An intuitive method is to switch on the N reflecting elements one-by-one and estimate each cascaded channel coefficient in a one-by-one manner [96]. Since an additional sub-phase is needed to estimate the direct BS-UE channel with all the elements off, $N + 1$ sub-phases are required. To reduce this large overhead, the ON/OFF scheme has been modified in [97] by adopting an element grouping method, where a sub-surface consisting of neighboring elements is turned on in each estimation sub-phase. In [98], the entire RIS is switched on in each sub-phase by applying discrete Fourier transform sequences. Moreover, a three-phase channel estimation framework has been proposed in [99] by exploiting the correlations among the UE-RIS-BS cascade channels of different users. On the one hand, these ON/OFF estimation methods impose a large pilot overhead due to the multiple training sub-phases and prohibitive power consumption since the reflecting elements are switched on/off frequently. On the other hand, it is difficult to ensure the channel estimation accuracy because only a part of the RIS is switched on in each sub-phase while all RIS elements are used for data transmissions.

To achieve separate channel estimation, an alternative RIS channel estimation framework based on

Table 2 RIS channel estimation

RIS structure	Channel estimation framework	Ref.	Pros	Cons
Passive RIS	ON/OFF	[96–99]	Low computational complexity	Excessive pilot overhead and prohibitive power consumption
	Matrix decomposition	[100–104]	Low pilot overhead	Only for sparse RIS channels
Semi-passive RIS	Hybrid RIS	[105–108]	Reduced overhead for channel estimation	Additional hardware cost
	Deep learning	[109]	Integrated RIS reflection design with channel estimation	Additional hardware cost

matrix decomposition has recently gained attention. In [100], a bilinear generalized approximate message passing (BiG-AMP) algorithm has been adopted for sparse channel matrix decomposition. Further in [101], the channel estimation and the RIS-related activity detection problems have been jointly solved by the BiG-AMP, singular value thresholding, and vector AMP algorithms. In addition, parallel factor decomposition has been considered as an efficient method for estimating RIS-assisted massive MIMO channels [102–104]. This algorithm reduces the complexity of low-rank matrix estimations via decomposing a high dimensional matrix into a linear combination of multiple rank-one tensors. Note that the efficiency of matrix decomposition relies heavily on the sparsity of the RIS-assisted MIMO channels which restricts its applications to general scenarios except for high-frequency communications.

5.1.2 *Channel estimation for semi-passive RIS*

A passive RIS with no RF chains introduces negligible power consumption. However, as aforementioned, it is difficult for this passive architecture to obtain accurate CSI. Recently, low-power active sensors have been successfully installed at the RIS to trade off the channel estimation performance and hardware/energy cost. This semi-passive RIS structure with limited active sensors is different from the concept of active RIS discussed in Section 1, where each element is equipped with an amplifier.

For an RIS with a smaller number of active sensors than that of the reflecting elements, two different RIS architectures have been studied in [105–109]. One is similar to the structure of hybrid massive MIMO [110], called hybrid RIS [105,106], in which a cluster of adjacent reflecting elements are connected to the same RF chain, acting as a sub-surface. The phase shifts of all these reflecting elements in each sub-surface can be set either to the same or to a different state. For this structure, the BS-RIS and RIS-UE channels can be separately obtained by sending training pilots to the RIS from the BS and UEs [107]. Compared to purely passive RISs, the pilot overhead of this hybrid RIS is significantly reduced [108]. The other approach is to randomly choose some RIS reflecting elements connected to the active sensors while the others remain passive [109]. It is revealed that the full BS-RIS and RIS-UE channels can be recovered from the sampled channel coefficients sensed at the active elements via compressive sensing.

Despite the existing studies as summarized in Table 2, it is still an open problem to achieve accurate RIS channel estimation at an acceptable cost especially considering practical hardware impairments.

5.2 Interplay of RIS with deep learning

In order to serve multifarious applications for 6G by dynamically manipulating the wireless environments with RIS, it would be beneficial to utilize machine learning, especially deep learning (DL) technologies [111–113]. It is usually difficult to solve the joint optimization of RIS reflection and BS precoding due to the varying wireless environment, moving terminals, and the interactions between active and passive beamforming, especially with extra nonconvex constraints and practical hardware impairments. It has been revealed that DL methods can help solve complicated nonconvex optimization problems with better solutions at lower cost [114]. Recently, intensive efforts have been devoted to studying the interplay of RIS with DL techniques [43,115–124].

On the one hand, a typical way of exploiting DL for RIS-assisted wireless communication is to treat the entire transmission system as a black-box deep neural network (DNN) [115–117]. In such a data-driven DL framework, no expert knowledge of wireless environments or specific mathematical formulations is required. By using reinforcement learning with DL, the target action of RIS can be learned by observing instant rewards of trial-and-error interactions with the given state. In [118], deep reinforcement learning (DRL) has been adopted to jointly design the RIS reflection and BS precoding for multiuser MISO communications. This DRL-based technique has been extended to a multi-hop RIS-empowered system in [43]. To maximize the energy efficiency of a downlink multiuser MISO network, a DRL-based framework

has been proposed in [119] to jointly design the phase shifts at the RIS and the transmit power at the BS. Further to optimize the joint reflection of a plurality of RISs, a low-complexity supervised learning approach has been presented in [120]. Exploiting 1-bit phase shifters at the RIS, the reflection coefficients can be considered as a binary vector. For this practical deployment, a deep Q-network has been utilized to explore the binary action spaces [121]. In addition to the downlink transmissions studied in these aforementioned studies, for an RIS-assisted multiuser uplink framework, a DL-based approach has been proposed in [122] to jointly optimize the RIS reflection and symbol detection. Different from existing alternating optimization algorithms, DL/DRL-based solutions are appropriate to solving joint optimization problems since they can achieve multiple target variables simultaneously as the outputs of a DNN.

On the other hand, model-driven DL structures have recently attracted increasing attention. It is of great interest to construct DL networks which are inspired by mathematical models of RIS communication, including channel estimation, data detection, and beam management. Utilizing a portion of active reflecting elements equipped for channel acquisition, a DL-based channel estimation method has been proposed in [123]. The cascade channel through active elements is obtained via conventional pilot training while that through passive elements is predicted via a DNN. Based on deep unfolding, the authors of [124] have designed a model-driven DL detector for an RIS-aided spatial modulation system. It has been shown that the proposed DL detector outperforms the traditional greedy algorithm.

In general, the design of data-driven DNNs is a black-box strategy. However, the training overhead makes it difficult to meet the low latency and high mobility requirements of 6G. Compared to data-driven DNNs, the number of trainable parameters of model-driven networks can usually be significantly reduced, at the cost of sophisticated network design based on mathematical formulations. It is still an open problem to trade off system performance, network complexity, and training overhead for RIS and DL.

5.3 Hardware implementation of RIS

The performance gain of RIS is determined by the resolution of the reflecting elements [125]. A PIN diode is the most commonly used device to generate the phase shifts of RIS [126]. To be specific, discrete phase shifts are determined by the states of a cluster of PIN diodes with each diode switched on/off. A PIN diode provides a one-bit phase resolution [7]. The increment of phase resolution usually leads to an exponential growth of hardware cost, which is challenging, especially for RIS with a large number of reflecting elements.

In addition, RIS is dynamically controlled by a micro-controller and field-programmable gate array (FPGA) to generate the desired phase shifts for real-time communications. Due to the rapidly varying wireless environments and fast-moving terminals, the system performance with RIS is highly determined by the control response time of the reflecting elements. For practical implementations, it is difficult to improve the device response bandwidth which usually results in a dramatic increment of hardware cost and power consumption. Hence, it is an interesting problem to further consider tradeoffs between the RIS performance and the hardware cost in practical RIS deployments.

The multiplicative path loss of RIS, which acts as an inherently passive surface, inevitably leads to performance degradation especially when the RIS is located far from transceiver terminals. Minimal active devices have been exploited to alleviate the effect of double path loss. Particularly, a power amplifier has been incorporated with two RISs to form an amplifying RIS [127]. Compared to passive RIS-assisted systems, this architecture significantly improves the energy efficiency of wireless communications. In addition, some active devices can provide the ability of signal processing to further enhance the system performance at the cost of higher hardware and power consumption. The hardware design of RIS with minimal active devices is an important issue to be studied.

Despite the aforementioned challenges, the evolution of metamaterials provides great opportunities for the development of RIS. One newly emerging technology is to enable the RIS to perform mathematical calculations and artificial intelligence computations by adopting energy efficient computational metamaterials [128]. Based on this new hardware implementation, communication and computation can be efficiently integrated on RIS to meet the variety of requirements of 6G.

5.4 Holographic surface

The concept of holographic surface is arising as a new paradigm shift in RIS-assisted wireless communications. To be specific, a holographic surface consists of an ultra large number of tiny reflecting elements densely integrated in a compact surface to yield a spatially continuous (or quasi-continuous) aperture [129, 130]. In its asymptotic form, a holographic surface is considered to be equipped with an infinite number of elements separated by an infinitesimal spacing [131]. Compared to a conventional RIS, the effective reflection area of a holographic surface is larger, and thus, a higher fraction of energy of the incident signals can be reflected towards a desired direction. On the other hand, the sidelobe power leakage of a holographic surface is significantly suppressed compared to that of a critically-spaced RIS. Thanks to these advantages, some efforts have been devoted to investigating communication systems equipped with holographic surfaces. In [42], an effective baseband channel model has been mathematically formulated for a holographic RIS, and the beam pattern of the holographic RIS has also been analyzed in the context of a massive MIMO system. Utilizing the derived expressions for holographic beam patterns, two beamforming schemes of holographic RIS have been proposed for channel estimation and data transmission. In [132], the joint optimization of holographic beamforming and digital precoding has been studied to maximize the sum rate of a multiuser communication system. Moreover, the authors of [13] have investigated the spectral efficiency of a multiuser holographic MIMO communication system with MRT and zero-forcing precoding. It is revealed that the spectral efficiency increases when more elements separated by a fixed spacing are available at the holographic transmitter and receiver.

Despite these available studies, there are still multiple key challenges for transceiver design of holographic surfaces. On the one hand, it is still challenging to acquire the CSI of a holographic surface composed of an ultra large number of elements. On the other hand, the element spacing of a holographic surface is an important design parameter to be optimized. Specifically, a narrower beamforming can be obtained to achieve better performance by a holographic surface with smaller element spacing. However, when the element spacing decreases, mutual coupling effects between adjacent elements become stronger and the signal correlations correspondingly increase, leading to inevitable performance degradation if not taken into account by design.

6 Conclusion

In this study, we provided an overview on RIS-based techniques, motivated by the emerging consideration of RISs as a key enabling technology for 6G networks. Specifically, we elaborated on two core functionalities of RIS, i.e., reflection and modulation, as well as their substantial benefits to wireless communication systems. Then, we presented the application of RIS to 6G networks. To meet the prominent requirement of secure communications, we discussed how to enhance physical-layer security in terms of secrecy rate and SOP. In particular, we proposed a typical case study exemplifying the benefits of RISs to secure communications. Both theoretical analysis and simulation results demonstrated the beneficial impact of RISs on the ergodic secrecy rate. Finally, we listed a multitude of challenges and open opportunities in order to reap the full potentials of RISs. We hope that this overview provides a useful guide for further research in the field of RIS-assisted wireless communications.

Acknowledgements This work was supported in part by Ministry of Education, Singapore, under its MOE Tier 2 (Grant No. MOE-T2EP50220-0019), EU H2020 RISE-6G project (Grant No. 10101701), National Key R&D Program of China (Grant No. 2021YFA1000500), National Natural Science Foundation of China (Grant No. 62101492), Zhejiang Provincial Natural Science Foundation of China (Grant No. LR22F010002), National Natural Science Fund for Excellent Young Scientists Fund Program (Overseas), Zhejiang University Education Foundation Qizhen Scholar Foundation, and Fundamental Research Funds for the Central Universities (Grant No. 2021FZZX001-21). The work of M. DI RENZO was supported in part by the European Commission through H2020 ARIADNE Project (Grant No. 871464) and through H2020 RISE-6G Project (Grant No. 101017011). Any opinions, findings and conclusion or recommendations expressed in this material are those of the authors and do not reflect the views of the Ministry of Education, Singapore.

References

1 Zhang L, Liang Y C, Niyato D. 6G visions: mobile ultra-broadband, super Internet-of-Things, and artificial intelligence. China Commun, 2019, 16: 1–14
2 Wang C-X, Wu S B, Bai L, et al. Recent advances and future challenges for massive MIMO channel measurements and models. Sci China Inf Sci, 2016, 59: 021301
3 Xu J D, Xu W, Gong F K, et al. Optimal multiuser loading in quantized massive MIMO under spatially correlated channels. IEEE Trans Veh Technol, 2019, 68: 1459–1471

4 Xu J D, Xu W, Gong F K. On performance of quantized transceiver in multiuser massive MIMO downlinks. IEEE Wireless Commun Lett, 2017, 6: 562–565
5 Alexandropoulos G C, Lerosey G, Debbah M, et al. Reconfigurable intelligent surfaces and metamaterials: the potential of wave propagation control for 6G wireless communications. IEEE Comsoc TCCN Newsletter, 2020, 6: 1–9
6 Jian M N, Alexandropoulos G C, Basar E, et al. Reconfigurable intelligent surfaces for wireless communications: overview of hardware designs, channel models, and estimation techniques. Intell Converged Netw, 2022, 3: 1–32
7 Liang Y-C, Chen J, Long R Z, et al. Reconfigurable intelligent surfaces for smart wireless environments: channel estimation, system design and applications in 6G networks. Sci China Inf Sci, 2021, 64: 200301
8 Renzo M D, Zappone A, Debbah M, et al. Smart radio environments empowered by reconfigurable intelligent surfaces: how it works, state of research, and the road ahead. IEEE J Sel Areas Commun, 2020, 38: 2450–2525
9 Pan C H, Zhou G, Zhi K D, et al. An overview of signal processing techniques for RIS/IRS-aided wireless systems. IEEE J Sel Top Signal Process, 2022, 16: 883–917
10 Albanese A, Devoti F, Sciancalepore V, et al. MARISA: a self-configuring metasurfaces absorption and reflection solution towards 6G. In: Proceedings of IEEE Conference on Computer Communications, London, 2022. 250–259
11 Alexandropoulos G C, Shlezinger N, Hougne P D. Reconfigurable intelligent surfaces for rich scattering wireless communications: recent experiments, challenges, and opportunities. IEEE Commun Mag, 2021, 59: 28–34
12 You L, Xu J, Alexandropoulos G C, et al. Energy efficiency maximization of massive MIMO communications with dynamic metasurface antennas. IEEE Trans Wireless Commun, 2022. doi: 10.1109/TWC.2022.3194070
13 Wei L, Huang C W, Alexandropoulos G C, et al. Multi-user holographic MIMO surfaces: channel modeling and spectral efficiency analysis. IEEE J Sel Top Signal Process, 2022, 16: 1112–1124
14 Strinati E C, Alexandropoulos G C, Wymeersch H, et al. Reconfigurable, Intelligent, and Sustainable Wireless Environments for 6G Smart Connectivity. IEEE Commun Mag, 2021, 59: 99–105
15 Strinati E C, Alexandropoulos G, Sciancalepore V, et al. Wireless environment as a service enabled by reconfigurable intelligent surfaces: the RISE-6G perspective. In: Proceedings of Joint European Conference on Networks and Communications & 6G Summit (EuCNC/6G Summit), Porto, 2021. 1–6
16 Alexandropoulos G C, Crozzoli M, Phan-Huy D-T, et al. Smart wireless environments enabled by RISs: deployment scenarios and two key challenges. In: Proceedings of Joint European Conference on Networks and Communications & 6G Summit (EuCNC/6G Summit), Grenoble, 2022. 1–6
17 You L, Xiong J Y, Ng D W K, et al. Energy efficiency and spectral efficiency tradeoff in RIS-aided multiuser MIMO uplink transmission. IEEE Trans Signal Process, 2020, 69: 1407–1421
18 Huang C W, Zappone A, Alexandropoulos G C, et al. Reconfigurable intelligent surfaces for energy efficiency in wireless communication. IEEE Trans Wireless Commun, 2019, 18: 4157–4170
19 Zhou S, Xu W, Wang K, et al. Spectral and energy efficiency of IRS-assisted MISO communication with hardware impairments. IEEE Wireless Commun Lett, 2020, 9: 1366–1369
20 Di B, Zhang H L, Song L Y, et al. Hybrid beamforming for reconfigurable intelligent surface based multi-user communications: achievable rates with limited discrete phase shifts. IEEE J Sel Areas Commun, 2020, 38: 1809–1822
21 Yang L, Yang Y, Hasna M O, et al. Coverage, probability of SNR gain, and DOR analysis of RIS-aided communication systems. IEEE Wireless Commun Lett, 2020, 9: 1268–1272
22 van Chien T, Tu L T, Chatzinotas S, et al. Coverage probability and ergodic capacity of intelligent reflecting surface-enhanced communication systems. IEEE Commun Lett, 2021, 25: 69–73
23 He M X, Xu J D, Xu W, et al. RIS-assisted quasi-static broad coverage for wideband mmWave massive MIMO systems. 2022. ArXiv:2203.00400
24 Shen H, Xu W, Gong S L, et al. Secrecy rate maximization for intelligent reflecting surface assisted multi-antenna communications. IEEE Commun Lett, 2019, 23: 1488–1492
25 Xiu Y, Zhao J, Yuen C, et al. Secure beamforming for multiple intelligent reflecting surfaces aided mmWave systems. IEEE Commun Lett, 2010, 25: 417–421
26 Hong S, Pan C H, Ren H, et al. Artificial-noise-aided secure MIMO wireless communications via intelligent reflecting surface. IEEE Trans Commun, 2020, 68: 7851–7866
27 Yu X H, Xu D F, Sun Y, et al. Robust and secure wireless communications via intelligent reflecting surfaces. IEEE J Sel Areas Commun, 2020, 38: 2637–2652
28 Alexandropoulos G C, Katsanos K, Wen M W, et al. Safeguarding MIMO communications with reconfigurable metasurfaces and artificial noise. In: Proceedings of IEEE International Conference on Communications (ICC), Montreal, 2021. 1–6
29 Yang L, Yang J X, Xie W W, et al. Secrecy performance analysis of RIS-aided wireless communication systems. IEEE Trans Veh Technol, 2020, 69: 12296–12300
30 Zhang J Y, Du H Y, Sun Q, et al. Physical layer security enhancement with reconfigurable intelligent surface-aided networks. IEEE Trans Inform Forensic Secur, 2021, 16: 3480–3495
31 Trigui I, Ajib W, Zhu W P. Secrecy outage probability and average rate of RIS-aided communications using quantized phases. IEEE Commun Lett, 2021, 25: 1820–1824
32 Cao X L, Yang B, Huang C W, et al. AI-assisted MAC for reconfigurable intelligent-surface-aided wireless networks: challenges and opportunities. IEEE Commun Mag, 2021, 59: 21–27
33 Cao X L, Yang B, Zhang H L, et al. Reconfigurable-intelligent-surface-assisted MAC for wireless networks: protocol design, analysis, and optimization. IEEE Internet Things J, 2021, 8: 14171–14186
34 Bao V N Q, Duong T Q, da Costa D B, et al. Cognitive amplify-and-forward relaying with best relay selection in non-identical rayleigh fading. IEEE Commun Lett, 2013, 17: 475–478
35 Ho-Van K, Sofotasios P C, Alexandropoulos G C, et al. Bit error rate of underlay decode-and-forward cognitive networks with best relay selection. J Commun Netw, 2015, 17: 162–171
36 Liu J, Xu J D, Xu W, et al. Multiuser massive MIMO relaying with mixed-ADC receiver. IEEE Signal Process Lett, 2016, 24: 76–80
37 Zhang Z J, Dai L L, Chen X B, et al. Active RIS vs. passive RIS: which will prevail in 6G? 2022. ArXiv:2103.15154
38 Long R Z, Liang Y C, Pei Y Y, et al. Active reconfigurable intelligent surface-aided wireless communications. IEEE Trans Wireless Commun, 2021, 20: 4962–4975
39 Akdeniz M R, Liu Y, Samimi M K, et al. Millimeter wave channel modeling and cellular capacity evaluation. IEEE J Sel Areas Commun, 2014, 32: 1164–1179
40 Xu J D, Xu W, Zhang H, et al. Performance analysis of multi-cell millimeter-wave massive MIMO networks with low-precision

ADCs. IEEE Trans Commun, 2019, 67: 302–317
41 Xiu Y, Zhao J, Sun W, et al. Secrecy rate maximization for reconfigurable intelligent surface aided millimeter wave system with low-resolution DACs. IEEE Commun Lett, 2021, 25: 2166–2170
42 Wan Z W, Gao Z, Gao F F, et al. Terahertz massive MIMO with holographic reconfigurable intelligent surfaces. IEEE Trans Commun, 2021, 69: 4732–4750
43 Huang C W, Yang Z H, Alexandropoulos G C, et al. Multi-hop RIS-empowered terahertz communications: a DRL-based hybrid beamforming design. IEEE J Sel Areas Commun, 2021, 39: 1663–1677
44 Xu J D, Xu W, Zhang H, et al. Asymmetrically reconstructed optical OFDM for visible light communications. IEEE Photonics J, 2016, 8: 1–18
45 Yang L, Yan X Q, da Costa D B, et al. Indoor mixed dual-hop VLC/RF systems through reconfigurable intelligent surfaces. IEEE Wireless Commun Lett, 2020, 9: 1995–1999
46 Abumarshoud H, Mohjazi L, Dobre O A, et al. LiFi through reconfigurable intelligent surfaces: a new frontier for 6G? IEEE Veh Technol Mag, 2022, 17: 37–46
47 Keykhosravi K, Denis B, Alexandropoulos G C, et al. Leveraging RIS-enabled smart signal propagation for solving infeasible localization problems. 2022. ArXiv:2204.11538
48 Zhang H B, Zhang H L, Di B, et al. Holographic integrated sensing and communication. IEEE J Sel Areas Commun, 2022, 40: 2114–2130
49 Shi W, Xu W, You X, et al. Intelligent reflection enabling technologies for integrated and green Internet-of-Everything beyond 5G: communication, sensing, and security. IEEE Wireless Commun, 2022. doi: 10.1109/MWC.018.2100717
50 Cao X L, Yang B, Huang C W, et al. Converged reconfigurable intelligent surface and mobile edge computing for space information networks. IEEE Network, 2021, 35: 42–48
51 Merluzzi M, Costanzo F, Katsanos K D, et al. Power minimizing MEC offloading with probabilistic QoS constraints for RIS-empowered communication systems. In: Proceedings of IEEE Global Communications Conference (GLOBECOM), Rio de Janeiro, 2022. 1–6
52 Cao X L, Yang B, Huang C W, et al. Massive access of static and mobile users via reconfigurable intelligent surfaces: protocol design and performance analysis. IEEE J Sel Areas Commun, 2022, 40: 1253–1269
53 Qi Q, Chen X M, Zhong C J, et al. Physical layer security for massive access in cellular Internet of Things. Sci China Inf Sci, 2020, 63: 121301
54 Xu J D, Xu W, Zhu J, et al. Secure massive MIMO communication with low-resolution DACs. IEEE Trans Commun, 2019, 67: 3265–3278
55 Lv L, Li Z, Ding H Y, et al. Secure coordinated direct and untrusted relay transmissions via interference engineering. Sci China Inf Sci, 2022, 65: 182304
56 Teng Y, Li J Y, Huang M X, et al. Low-complexity and high-performance receive beamforming for secure directional modulation networks against an eavesdropping-enabled full-duplex attacker. Sci China Inf Sci, 2022, 65: 119302
57 Shannon C E. Communication theory of secrecy systems. Bell Syst Technical J, 1949, 28: 656–715
58 Xu J D, Xu W, Ng D W K, et al. Secure communication for spatially sparse millimeter-wave massive MIMO channels via hybrid precoding. IEEE Trans Commun, 2020, 68: 887–901
59 Zhou G, Pan C H, Ren H, et al. Robust beamforming design for intelligent reflecting surface aided MISO communication systems. IEEE Wireless Commun Lett, 2020, 9: 1658–1662
60 Zhou G, Pan C H, Ren H, et al. A framework of robust transmission design for IRS-aided MISO communications with imperfect cascaded channels. IEEE Trans Signal Process, 2020, 68: 5092–5106
61 Wei L, Huang C W, Guo Q H, et al. Joint channel estimation and signal recovery for RIS-empowered multiuser communications. IEEE Trans Commun, 2022, 70: 4640–4655
62 Zhao Y Q, Xu W, You X H, et al. Cooperative reflection and synchronization design for distributed multiple-RIS communications. IEEE J Sel Top Signal Process, 2022, 16: 980–994
63 Han Y, Tang W K, Jin S, et al. Large intelligent surface-assisted wireless communication exploiting statistical CSI. IEEE Trans Veh Technol, 2019, 68: 8238–8242
64 Peng Z J, Li T S, Pan C H, et al. Analysis and optimization for RIS-aided multi-pair communications relying on statistical CSI. IEEE Trans Veh Technol, 2021, 70: 3897–3901
65 Gao Y W, Xu J D, Xu W, et al. Distributed IRS with statistical passive beamforming for MISO communications. IEEE Wireless Commun Lett, 2021, 10: 221–225
66 Hu X L, Wang J W, Zhong C J. Statistical CSI based design for intelligent reflecting surface assisted MISO systems. Sci China Inf Sci, 2020, 63: 222303
67 Dang J, Zhang Z C, Wu L. Joint beamforming for intelligent reflecting surface aided wireless communication using statistical CSI. China Commun, 2020, 17: 147–157
68 Zhao M M, Wu Q Q, Zhao M J, et al. Intelligent reflecting surface enhanced wireless networks: two-timescale beamforming optimization. IEEE Trans Wireless Commun, 2021, 20: 2–17
69 Li Q, Wen M W, Renzo M D. Single-RF MIMO: from spatial modulation to metasurface-based modulation. IEEE Wireless Commun, 2021, 28: 88–95
70 Karasik R, Simeone O, Renzo M D, et al. Adaptive coding and channel shaping through reconfigurable intelligent surfaces: an information-theoretic analysis. IEEE Trans Commun, 2021, 69: 7320–7334
71 Guo S S, Lv S H, Zhang H X, et al. Reflecting modulation. IEEE J Sel Areas Commun, 2020, 38: 2548–2561
72 Cheng H V, Yu W. Degree-of-freedom of modulating information in the phases of reconfigurable intelligent surface. 2021. ArXiv:2112.13787
73 Yan W J, Yuan X J, He Z-Q, et al. Passive beamforming and information transfer design for reconfigurable intelligent surfaces aided multiuser MIMO systems. IEEE J Sel Areas Commun, 2020, 38: 1793–1808
74 Lin S, Zheng B X, Alexandropoulos G C, et al. Reconfigurable intelligent surfaces with reflection pattern modulation: beamforming design and performance analysis. IEEE Trans Wireless Commun, 2021, 20: 741–754
75 Lin S, Chen F J, Wen M W, et al. Reconfigurable intelligent surface-aided quadrature reflection modulation for simultaneous passive beamforming and information transfer. IEEE Trans Wireless Commun, 2022, 21: 1469–1481
76 Yuan J, Wen M W, Li Q, et al. Receive quadrature reflecting modulation for RIS-empowered wireless communications. IEEE Trans Veh Technol, 2021, 70: 5121–5125
77 Tang W K, Dai J Y, Chen M Z, et al. MIMO transmission through reconfigurable intelligent surface: system design, analysis, and implementation. IEEE J Sel Areas Commun, 2020, 38: 2683–2699

78 Elzanaty A, Guerra A, Guidi F, et al. Reconfigurable intelligent surfaces for localization: position and orientation error bounds. IEEE Trans Signal Process, 2021, 69: 5386–5402
79 Wang Z Y, Liu Z Y, Shen Y, et al. Location awareness in beyond 5G networks via reconfigurable intelligent surfaces. IEEE J Sel Areas Commun, 2022, 40: 2011–2025
80 Chen-Hu K, Alexandropoulos G C, Armada A G. Differential data-aided beam training for RIS-empowered multi-antenna communications. 2022. ArXiv:2204.13029
81 Chen-Hu K, Alexandropoulos G C, Armada A G. Non-coherent modulation with random phase configurations in RIS-empowered cellular MIMO systems. ITU J Future Evolving Technol, 2022, 3: 374–387
82 Song X X, Zhao D, Hua H C, et al. Joint transmit and reflective beamforming for IRS-assisted integrated sensing and communication. 2021. ArXiv:2111.13511
83 Liu R, Li M, Swindlehurst A L. Joint beamforming and reflection design for RIS-assisted ISAC systems. 2022. ArXiv:2203.00265
84 Yang B, Cao X L, Huang C W, et al. Intelligent spectrum learning for wireless networks with reconfigurable intelligent surfaces. IEEE Trans Veh Technol, 2021, 70: 3920–3925
85 Yang B, Cao X L, Huang C W, et al. Federated spectrum learning for reconfigurable intelligent surfaces-aided wireless edge networks. IEEE Trans Wireless Commun, 2022, 21: 9610–9626
86 Yang B, Cao X L, Huang C W, et al. Spectrum-learning-aided reconfigurable intelligent surfaces for "Green" 6G networks. IEEE Network, 2021, 35: 20–26
87 Song Q H, Zeng Y, Xu J, et al. A survey of prototype and experiment for UAV communications. Sci China Inf Sci, 2021, 64: 140301
88 Cao X L, Yang B, Huang C W, et al. Reconfigurable intelligent surface-assisted aerial-terrestrial communications via multi-task learning. IEEE J Sel Areas Commun, 2021, 39: 3035–3050
89 Cheng Y J, Peng W, Huang C W, et al. RIS-aided wireless communications: extra degrees of freedom via rotation and location optimization. IEEE Trans Wireless Commun, 2022, 21: 6656–6671
90 Guo H Z, Li J Y, Liu J J, et al. A survey on space-air-ground-sea integrated network security in 6G. IEEE Commun Surv Tutorials, 2022, 24: 53–87
91 Yang J, Johansson T. An overview of cryptographic primitives for possible use in 5G and beyond. Sci China Inf Sci, 2020, 63: 220301
92 Li G Y, Sun C, Xu W, et al. On maximizing the sum secret key rate for reconfigurable intelligent surface-assisted multiuser systems. IEEE Trans Inform Forensic Secur, 2022, 17: 211–225
93 Csiszar I, Körner J. Broadcast channels with confidential messages. IEEE Trans Inform Theor, 1978, 24: 339–348
94 Huang C, Xu J D, Zhang W H, et al. Semi-blind channel estimation for RIS-assisted MISO systems using expectation maximization. IEEE Trans Veh Technol, 2022, 71: 10173–10178
95 An J C, Wu Q Q, Yuen C. Scalable channel estimation and reflection optimization for reconfigurable intelligent surface-enhanced OFDM systems. IEEE Wireless Commun Lett, 2022, 11: 796–800
96 Mishra D, Johansson H. Channel estimation and low-complexity beamforming design for passive intelligent surface assisted MISO wireless energy transfer. In: Proceedings of IEEE International Conference on Acoustics, Speech and Signal Processing (ICASSP), Brighton, 2019. 1–5
97 You C S, Zheng B X, Zhang R. Channel estimation and passive beamforming for intelligent reflecting surface: discrete phase shift and progressive refinement. IEEE J Sel Areas Commun, 2020, 38: 2604–2620
98 Nadeem Q U A, Alwazani H, Kammoun A, et al. Intelligent reflecting surface-assisted multi-user MISO communication: channel estimation and beamforming design. IEEE Open J Commun Soc, 2020, 1: 661–680
99 Wang Z R, Liu L, Cui S G. Channel estimation for intelligent reflecting surface assisted multiuser communications: framework, algorithms, and analysis. IEEE Trans Wireless Commun, 2020, 19: 6607–6620
100 He Z Q, Yuan X J. Cascaded channel estimation for large intelligent metasurface assisted massive MIMO. IEEE Wireless Commun Lett, 2020, 9: 210–214
101 Xia S H, Shi Y M. Intelligent reflecting surface for massive device connectivity: joint activity detection and channel estimation. In: Proceedings of IEEE International Conference on Acoustics, Speech and Signal Processing (ICASSP), Barcelona, 2020. 5175–5179
102 Araujo G T D, Almeida A L F D. PARAFAC-based channel estimation for intelligent reflective surface assisted MIMO system. In: Proceedings of IEEE Sensor Array Multichannel Signal Process, Hangzhou, 2020. 1–6
103 Wei L, Huang C W, Alexandropoulos G C, et al. Channel estimation for RIS-empowered multi-user MISO wireless communications. IEEE Trans Commun, 2021, 69: 4144–4157
104 Yuan J, Alexandropoulos G C, Kofidis E, et al. Channel tracking for RIS-enabled multi-user SIMO systems in time-varying wireless channels. In: Proceedings of IEEE International Conference on Communications (ICC), Seoul, 2022. 1–6
105 Alexandropoulos G C, Shlezinger N, Alamzadeh I, et al. Hybrid reconfigurable intelligent metasurfaces: enabling simultaneous tunable reflections and sensing for 6G wireless communications. 2021. ArXiv:2104.04690
106 Alamzadeh I, Alexandropoulos G C, Shlezinger N, et al. A reconfigurable intelligent surface with integrated sensing capability. Sci Rep, 2021, 11: 1–10
107 Alexandropoulos G C, Vlachos E. A hardware architecture for reconfigurable intelligent surfaces with minimal active elements for explicit channel estimation. In: Proceedings of IEEE International Conference on Acoustics, Speech, and Signal Processing, Barcelona, 2020. 9175–9179
108 Zhang H Y, Shlezinger N, Alexandropoulos G C, et al. Channel estimation with hybrid reconfigurable intelligent metasurfaces. 2022. ArXiv:2206.03913
109 Taha A, Alrabeiah M, Alkhateeb A. Enabling large intelligent surfaces with compressive sensing and deep learning. IEEE Access, 2021, 9: 44304–44321
110 Xu J D, Wang Y C, Xu W, et al. On uplink performance of multiuser massive MIMO relay network with limited RF chains. IEEE Trans Veh Technol, 2020, 69: 8670–8683
111 Renzo M D, Debbah M, Phan-Huy D T, et al. Smart radio environments empowered by reconfigurable AI meta-surfaces: an idea whose time has come. J Wireless Com Network, 2019, 2019: 129
112 Alexandropoulos G C, Stylianopoulos K, Huang C, et al. Pervasive machine learning for smart radio environments enabled by reconfigurable intelligent surfaces. Proc IEEE, 2022, 110: 1494–1525
113 Xu W, Yang Z H, Ng D W K, et al. Edge learning for B5G networks with distributed signal processing: semantic communication, edge computing, and wireless sensing. 2022. ArXiv:2206.00422

114 You X H, Zhang C, Tan X S, et al. AI for 5G: research directions and paradigms. Sci China Inf Sci, 2019, 62: 021301
115 Huang C W, Alexandropoulos G C, Yuen C, et al. Indoor signal focusing with deep learning designed reconfigurable intelligent surfaces. In: Proceedings of IEEE International Workshop on Signal Processing Advances in Wireless Communications, Cannes, 2019. 1–6
116 Stylianopoulos K, Alexandropoulos G C, Huang C W, et al. Deep contextual bandits for orchestrating multi-user MISO systems with multiple RISs. In: Proceedings of IEEE International Conference on Communications (ICC), Seoul, 2022. 1–6
117 Stylianopoulos K, Shlezinger N, Hougne P D, et al. Deep-learning-assisted configuration of reconfigurable intelligent surfaces in dynamic rich-scattering environments. In: Proceedings of IEEE International Conference on Acoustics, Speech, and Signal Processing, Singapore, 2022. 1–5
118 Huang C W, Mo R H, Yuen C. Reconfigurable intelligent surface assisted multiuser MISO systems exploiting deep reinforcement learning. IEEE J Sel Areas Commun, 2020, 38: 1839–1850
119 Lee G, Jung M, Kasgari A T Z, et al. Deep reinforcement learning for energy-efficient networking with reconfigurable intelligent surfaces. In: Proceedings of IEEE International Conference on Communications (ICC), Dublin, 2020. 1–6
120 Alexandropoulos G C, Samarakoon S, Bennis M, et al. Phase configuration learning in wireless networks with multiple reconfigurable intelligent surfaces. In: Proceedings of IEEE Global Communications Conference (GLOBECOM), Taipei, 2020. 1–6
121 Stylianopoulos K, Alexandropoulos G C. Online RIS configuration learning for arbitrary large numbers of 1-bit phase resolution elements. In: Proceedings of IEEE International Workshop on Signal Processing Advances in Wireless Communications, Oulu, 2022. 1–6
122 Wang L H, Shlezinger N, Alexandropoulos G C, et al. Jointly learned symbol detection and signal reflection in RIS-aided multi-user MIMO systems. In: Proceedings of IEEE Asilomar Signals, Systems and Computer Conference, Pacific Grove, 2021. 1–7
123 Gao S, Dong P H, Pan Z W, et al. Deep multi-stage CSI acquisition for reconfigurable intelligent surface aided MIMO systems. IEEE Commun Lett, 2021, 25: 2024–2028
124 Liu J, Renzo D R. Data-driven and model-driven deep learning detection for RIS-aided spatial modulation. In: Proceedings of IEEE 4th 5G World Forum (5GWF), Montreal, 2021. 88–92
125 Fara R, Ratajczak P, Phan-Huy D T, et al. A prototype of reconfigurable intelligent surface with continuous control of the reflection phase. IEEE Wireless Commun, 2022, 29: 70–77
126 Abeywickrama S, Zhang R, Wu Q, et al. Intelligent reflecting surface: practical phase shift model and beamforming optimization. IEEE Trans Commun, 2020, 68: 5849–5863
127 Tasci R A, Kilinc F, Basar E, et al. A new RIS architecture with a single power amplifier: energy efficiency and error performance analysis. IEEE Access, 2022, 10: 44804–44815
128 Liu C S, Chen H W, Wang S Y, et al. Two-dimensional materials for next-generation computing technologies. Nat Nanotechnol, 2020, 15: 545–557
129 Huang C W, Hu S, Alexandropoulos G C, et al. Holographic MIMO surfaces for 6G wireless networks: opportunities, challenges, and trends. IEEE Wireless Commun, 2020, 27: 118–125
130 Xu J, You L, Alexandropoulos G C, et al. Near-field wideband extremely large-scale MIMO transmission with holographic metasurface antennas. 2022. ArXiv:2205.02533
131 Pizzo A, Marzetta T L, Sanguinetti L. Spatially-stationary model for holographic MIMO small-scale fading. IEEE J Sel Areas Commun, 2020, 38: 1964–1979
132 Deng R Q, Di B Y, Zhang H L, et al. Reconfigurable holographic surfaces for future wireless communications. IEEE Wireless Commun, 2021, 28: 126–131
133 Gradshteyn I S, Ryzhik I M. Table of Integrals, Series, and Products. Burlington: Academic Press, 2014
134 Abramowitz M, Stegun I A. Handbook of Mathematical Functions. New York: Martino Publishing, 2014

Appendix A Proof of Observation 1

Assuming $l_{\rm B} \geqslant l_{\rm E}$ in (7), we have

$$\begin{aligned}\mathbb{E}\{R_S\} &= \mathbb{E}\left\{\log_2\left(1+\frac{l_{\rm A}l_{\rm B}MN^2P}{\sigma_n^2}\right)-\log_2\left(1+\frac{l_{\rm A}l_{\rm E}MP}{\sigma_n^2}\left|\boldsymbol{g}_{\rm E}^{\rm H}\boldsymbol{g}_{\rm B}\right|^2\right)\right\}\\ &\geqslant \log_2\left(1+\frac{l_{\rm A}l_{\rm B}MN^2P}{\sigma_n^2}\right)-\log_2\left(1+\frac{l_{\rm A}l_{\rm E}MP}{\sigma_n^2}\mathbb{E}\left\{\left|\boldsymbol{g}_{\rm E}^{\rm H}\boldsymbol{g}_{\rm B}\right|^2\right\}\right) \quad \text{(A1)}\\ &\to \log_2\left(1+\frac{l_{\rm A}l_{\rm B}MN^2P}{\sigma_n^2}\right)-\log_2\left(1+\frac{l_{\rm A}l_{\rm E}MP}{\sigma_n^2}\eta\right), \quad \text{(A2)}\end{aligned}$$

where Eq. (A1) uses the Jensen's inequality and Eq. (A2) is obtained by applying the following Lemma A1.

Lemma A1. For two independent channel vectors $\boldsymbol{g}_{\rm B}$ and $\boldsymbol{g}_{\rm E}$, it follows for large N that

$$\mathbb{E}\left\{|\boldsymbol{g}_{\rm E}^{\rm H}\boldsymbol{g}_{\rm B}|^2\right\}\to\eta, \quad \text{(A3)}$$

where η is defined as $\eta \triangleq N-\frac{2}{\pi^2}(N-1)+\frac{2N}{\pi^2}(\ln N+a)$.

Proof. According to the expressions of $\boldsymbol{g}_{\rm B}$ and $\boldsymbol{g}_{\rm E}$, $\mathbb{E}\{|\boldsymbol{g}_{\rm E}^{\rm H}\boldsymbol{g}_{\rm B}|^2\}$ is evaluated as

$$\begin{aligned}\mathbb{E}\left\{|\boldsymbol{g}_{\rm E}^{\rm H}\boldsymbol{g}_{\rm B}|^2\right\} =& \mathbb{E}\left\{\sum_{n=0}^{N-1}\mathrm{e}^{\mathrm{j}n\pi(\cos\psi_{\rm E}-\cos\psi_{\rm B})}\times\sum_{n=0}^{N-1}\mathrm{e}^{-\mathrm{j}n\pi(\cos\psi_{\rm E}-\cos\psi_{\rm B})}\right\}\\ =& N+\sum_{n=1}^{N-1}(N-n)\times\left[\mathbb{E}\left\{\mathrm{e}^{\mathrm{j}n\pi(\cos\psi_{\rm E}-\cos\psi_{\rm B})}\right\}+\mathbb{E}\left\{\mathrm{e}^{-\mathrm{j}n\pi(\cos\psi_{\rm E}-\cos\psi_{\rm B})}\right\}\right]\end{aligned}$$

$$=N+\sum_{n=1}^{N-1}(N-n)\times\left[\mathbb{E}\left\{\mathrm{e}^{\mathrm{j}n\pi\cos\psi_{\mathrm{E}}}\right\}\mathbb{E}\left\{\mathrm{e}^{-\mathrm{j}n\pi\cos\psi_{\mathrm{B}}}\right\}+\mathbb{E}\left\{\mathrm{e}^{-\mathrm{j}n\pi\cos\psi_{\mathrm{E}}}\right\}\mathbb{E}\left\{\mathrm{e}^{\mathrm{j}n\pi\cos\psi_{\mathrm{B}}}\right\}\right] \tag{A4}$$

$$=N+2\sum_{n=1}^{N-1}(N-n)J_0^2(n\pi) \tag{A5}$$

$$\to N+2\sum_{n=1}^{N-1}\frac{N-n}{n\pi^2} \tag{A6}$$

$$=N-\frac{2}{\pi^2}(N-1)+\frac{2N}{\pi^2}\sum_{n=1}^{N-1}\frac{1}{n}$$

$$\to N-\frac{2}{\pi^2}(N-1)+\frac{2N}{\pi^2}(\ln N+a), \tag{A7}$$

where Eq. (A4) uses the fact that ψ_{E} is independent of ψ_{B} and Eq. (A5) exploits the equality

$$\mathbb{E}\left\{\mathrm{e}^{\mathrm{j}n\pi\cos\psi_{\mathrm{B}}}\right\}=\mathbb{E}\left\{\mathrm{e}^{-\mathrm{j}n\pi\cos\psi_{\mathrm{B}}}\right\}=\mathbb{E}\left\{\mathrm{e}^{\mathrm{j}n\pi\cos\psi_{\mathrm{E}}}\right\}=\mathbb{E}\left\{\mathrm{e}^{-\mathrm{j}n\pi\cos\psi_{\mathrm{E}}}\right\}=J_0(n\pi), \tag{A8}$$

where $J_\nu(\cdot)$ is the νth Bessel function. Take $\mathbb{E}\{\mathrm{e}^{\mathrm{j}n\pi\cos\psi_{\mathrm{B}}}\}$ for instance. Since ψ_{B} follows the uniform distribution $\mathrm{U}[0,\pi]$, we have

$$\begin{aligned}\mathbb{E}\left\{\mathrm{e}^{\mathrm{j}n\pi\cos\psi_{\mathrm{B}}}\right\}&=\mathbb{E}\left\{\cos(n\pi\cos\psi_{\mathrm{B}})+\mathrm{j}\sin(n\pi\cos\psi_{\mathrm{B}})\right\}\\&=\frac{1}{\pi}\int_0^\pi\cos(n\pi\cos\psi_{\mathrm{B}})\mathrm{d}\psi_{\mathrm{B}}+\frac{\mathrm{j}}{\pi}\int_0^\pi\sin(n\pi\cos\psi_{\mathrm{B}})\mathrm{d}\psi_{\mathrm{B}}\\&=J_0(n\pi),\end{aligned} \tag{A9}$$

where the last step is obtained by letting $m=0, z=n\pi$, and $x=\psi_{\mathrm{B}}$ in the integral equations

$$\int_0^\pi\cos(z\cos x)\cos mx\mathrm{d}x=\pi\cos\frac{m\pi}{2}J_m(z), \tag{A10}$$

and

$$\int_0^\pi\sin(z\cos x)\cos mx\mathrm{d}x=\pi\sin\frac{m\pi}{2}J_m(z), \tag{A11}$$

which are given in [133, Eqs. (18), (13), pp. 425]. The step in (A6) exploits the asymptotical result [134, Eq. 9.2.1]

$$J_\nu(x)\to\sqrt{\frac{2}{\pi x}}\cos\left(x-\frac{\nu\pi}{2}-\frac{\pi}{4}\right), \tag{A12}$$

for $|x|\to\infty$ with $\nu=0$. Note that the asymptotic equality in (A12) is tight even for small x. Finally, Eq. (A7) follows by large N and the definition of the Euler's constant [134] as

$$a\triangleq\lim_{n\to\infty}\left[\sum_{k=1}^{k=n-1}\frac{1}{k}-\ln n\right]. \tag{A13}$$